Energy Efficiency Maximization for RIS-UAVs Aided Communication Networks: A Joint Optimization Framework

Xinying Guo, Pupu Zhao, Jiankang Zhang, *Senior Member, IEEE*, Yi Song, and Sheng Chen, *Life Fellow, IEEE*

***Abstract*—In this letter, we propose an efficient resource allocation algorithm for communication systems assisted by multiple uncrewed aerial vehicles borne reconfigurable intelligent surfaces (RISs). The algorithm jointly optimizes the base station (BS) power allocation, active beamforming and RIS phase shifts to maximize the system energy efficiency (EE). As the EE maximization problem is a multi-variable coupling problem with non-convexity, we adopt a Dinkelbach-based block coordinate descent framework to decouple it into three subproblems. The BS power allocation and active beamforming subproblems are solved using fractional programming and Riemannian conjugate gradient algorithm, respectively. For the RIS phase shifts optimization, we propose a low-complexity momentum-accelerated coordinate descent algorithm. Numerical results validate the effectiveness of our joint optimization framework.**

***Index Terms*—Uncrewed aerial vehicle, reconfigurable intelligent surface, energy efficiency, power allocation, beamforming.**

I. Introduction

In THE rapid expansion of wireless communications, integrating reconfigurable intelligent surface with uncrewed aerial vehicle (RIS-UAV) as a relay offers a more reliable and energy-efficient solution for alleviating the load of ground cellular networks and improving communication quality [1]. Specifically, this approach combines the passive signal enhancement capability of RIS with the dynamic deployment flexibility of UAV, thereby effectively improving the adaptability and overall performance of communication systems [2]. Moreover, the path loss exponent in air-to-ground channels is typically lower than that for terrestrial connections [3]. Hence, RIS-UAV assisted systems exhibit superior performance in terms of coverage extension and transmission reliability.

However, how to enhance the RIS-UAV assisted system spectral efficiency (SE) while maximizing energy efficiency (EE) remains one of the key research challenges. In [4], the authors studied an aerial RIS-aided over-the-air federated learning system and proposed an effective resource allocation scheme to maximize the system EE. The work [5] employed a joint optimization approach for RIS phase shifts, user scheduling, power allocation and UAV trajectory, aiming to maximize the system EE. The study [6] adopted a deep reinforcement learning (DRL) based method to jointly optimize RIS phase shifts and UAV trajectory for maximizing the EE of a rotary-wing UAV. Nevertheless, most of the existing studies have focused on single RIS-UAV systems, which results in low-rank channel matrices, thereby limiting the achievable beamforming gain [7] and constraining further improvements in the system EE.

Received 24 April 2026; revised 1 July 2026; accepted 21 July 2026. Date of publication 27 July 2026; date of current version 6 August 2026. This work was supported in part by the National Natural Science Foundation of China under Grant 61901159 and Grant 62172141. The associate editor coordinating the review of this article and approving it for publication was Y. H. Kim. *(Corresponding author: Xinying Guo.)*

Xinying Guo, Pupu Zhao, and Yi Song are with the Key Laboratory of Grain Information Processing and Control, Ministry of Education, and the College of Information Science and Engineering, Henan University of Technology, Zhengzhou 450001, China (e-mail: guoxinying@haut.edu.cn; zpp2344@stu.haut.edu.cn; songyi@haut.edu.cn).

Jiankang Zhang is with the Department of Computing and Informatics, Bournemouth University, BH12 5BB Bournemouth, U.K. (e-mail: jzhang3@bournemouth.ac.uk).

Sheng Chen is with the School of Electronics and Computer Science, University of Southampton, SO17 1BJ Southampton, U.K. (e-mail: sqc@ecs.soton.ac.uk).

Digital Object Identifier 10.1109/LWC.2026.3717056

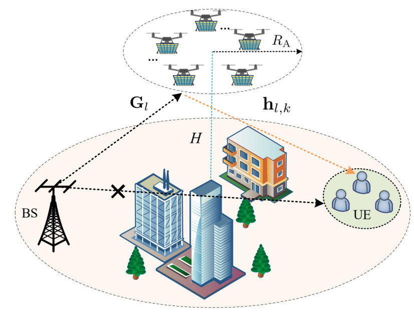

Fig. 1. Downlink multiuser communication system with the assistance of multiple RIS-UAVs.

RIS-UAVs communication networks, in contrast, can improve the aperture gain through an increased number of UAVs and create a rich scattering environment through diverse UAVs positions, enabling spatial multiplexing to serve numerous users [8]. In [8], a joint beamforming design was proposed that maximizes the system weighted sum rate by involving RIS phase shifts and UAVs positions. The work [7] adopted successive convex approximation and semi-definite programming (SDP) to jointly optimize the BS power allocation, active beamforming, RIS phase shifts and UAVs positions for maximizing the system sum rate, but the high computational complexity of SDP limits its scalability for large-scale RIS systems. Furthermore, these studies mainly focused on signal enhancement and rate improvement, without fully considering EE optimization. The authors in [9] employed a deep learning (DL) algorithm to jointly optimize the deployment of RIS-UAVs, on–off states of RIS reflecting elements, phase shifts and power control, in order to maximize the system EE. Although DL optimization algorithms perform excellently in fixed scenarios, due to the high training complexity, such algorithms are also difficult to adapt flexibly to various changes in practical applications.

To address the above challenges, this letter considers an RIS-UAVs assisted communication system with fixed RIS-UAVs positions scenario, formulating an EE maximization problem by joint design of BS power allocation, active beamforming and RIS phase shifts. Given the intrinsic non-convexity and inherent variable coupling of this joint optimization problem, we develop a solution framework based on Dinkelbach's method and block coordinate descent (BCD), which divides the original problem into three tractable subproblems. Specifically, fractional programming and Riemannian conjugate gradient method are employed to solve the subproblems of BS power allocation and active beamforming, respectively, while a low-complexity momentum-accelerated coordinate descent (MACD) algorithm is developed to optimize RIS phase shifts. Simulation results confirm significant EE gains over several baseline methods.

II. RIS-UAVs Aided Communication Network

A. Network Model

Fig. 1 depicts the downlink communication model of the RIS-UAVs assisted multi-user equipment (UE) system. Due to obstacles, such as high-rise buildings, direct link between the BS and the UEs may be blocked. L RIS-UAVs, indexed by the set $\mathcal{S}_{\mathrm{A}}=\{1,\ldots,L\}$, are deployed in the system to relay communications for K single-antenna UEs. Every RIS-UAV is equipped with $M = M_x \times M_y$ reflecting elements arranged in a uniform planar array, where the element spacing $d_{\mathrm{R}} < \lambda$ and λ is the carrier wavelength. The L RIS-UAVs are spread uniformly across a circular region of radius R_{A}, all at the same altitude H. The horizontal coordinate of the lth RIS-UAV is denoted by $\mathbf{q}_l = [x_l, y_l]^{\mathrm{T}}$, where $l \in \mathcal{S}_{\mathrm{A}}$.

The BS deploys N antennas in a uniform linear array with spacing $d_{\mathrm{B}} < \lambda$, and operates at a maximum transmission power $P_{\max}$. The distance between the BS and the lth RIS-UAV is $d_l = \sqrt{\|\mathbf{q}_l - \mathbf{q}_{\mathrm{B}}\|^2 + H^2}$, where $\mathbf{q}_{\mathrm{B}} = [x_{\mathrm{B}}, y_{\mathrm{B}}]^{\mathrm{T}}$ represents the horizontal coordinate of the BS. Within a circular region of radius R_{U}, K UEs are randomly distributed and indexed by the set $\mathcal{S}_{\mathrm{U}} = \{1,\ldots,K\}$. For each UE $k \in \mathcal{S}_{\mathrm{U}}$ with horizontal coordinate $\mathbf{q}_k = [x_k, y_k]^{\mathrm{T}}$, its distance to the lth RIS-UAV is given by $d_{l,k} = \sqrt{\|\mathbf{q}_l - \mathbf{q}_k\|^2 + H^2}$.

B. Channel Model

The lth RIS-UAV's receive array response vector and the BS's transmit array response vector are respectively given by

$$\mathbf{a}_{\mathrm{RU}}(r_l) = \Big[1,\, \mathrm{e}^{-j\frac{2\pi d_{\mathrm{R}}}{\lambda}(r_{l,x}+r_{l,y})},\, \ldots,\, \mathrm{e}^{-j\frac{2\pi d_{\mathrm{R}}}{\lambda}(M-1)(r_{l,x}+r_{l,y})}\Big]^{\mathrm{T}}, \tag{1}$$

$$\mathbf{a}_{\mathrm{BS}}(s) = \Big[1,\, \mathrm{e}^{-j\frac{2\pi d_{\mathrm{B}}}{\lambda}s},\, \ldots,\, \mathrm{e}^{-j\frac{2\pi d_{\mathrm{B}}}{\lambda}(N-1)s}\Big]^{\mathrm{T}}, \tag{2}$$

where $r_{l,x} = \sin(\phi_{l,1})\sin(\phi_{l,2})$ and $r_{l,y} = \cos(\phi_{l,1})\sin(\phi_{l,2})$, with $\phi_{l,1}$ and $\phi_{l,2}$ denoting the azimuth angle of arrival and elevation angle of arrival from the BS to the lth RIS-UAV, respectively, while s represents the cosine of the BS's angle of departure (AoD). Similarly, the transmit array response vector of the lth RIS-UAV is expressed as

$$\mathbf{a}_{\mathrm{RU}}(v_{l,k}) = \Big[1,\, \mathrm{e}^{-j\frac{2\pi d_{\mathrm{R}}}{\lambda}(v_{l,k,x}+v_{l,k,y})},\, \ldots,\, \mathrm{e}^{-j\frac{2\pi d_{\mathrm{R}}}{\lambda}(M-1)(v_{l,k,x}+v_{l,k,y})}\Big]^{\mathrm{T}}, \tag{3}$$

where $v_{l,k,x} = \sin(\phi_{l,k,1})\sin(\phi_{l,k,2})$ and $v_{l,k,y} = \cos(\phi_{l,k,1})\sin(\phi_{l,k,2})$, with $\phi_{l,k,1}$ and $\phi_{l,k,2}$ being the azimuth AoD and elevation AoD from the lth RIS-UAV to the kth UE. We assume that the necessary channel state information can be acquired by the method presented in [10]. Since both the line-of-sight (LoS) and non-line-of-sight (NLoS) propagations are presented in the BS-RIS and RIS-UE links, the use of the Rician fading model is justified, where the equivalent baseband channels from the BS to the lth RIS-UAV and from the lth RIS-UAV to the kth UE are respectively given by

$$\mathbf{G}_l = \sqrt{\tau d_l^{-\kappa}}\left(\sqrt{\frac{R}{R+1}}\,\bar{\mathbf{G}}_l + \sqrt{\frac{1}{R+1}}\,\tilde{\mathbf{G}}_l\right) \in \mathbb{C}^{M\times N}, \tag{4}$$

$$\mathbf{h}_{l,k} = \sqrt{\tau d_{l,k}^{-\kappa}}\left(\sqrt{\frac{R}{R+1}}\,\bar{\mathbf{h}}_{l,k} + \sqrt{\frac{1}{R+1}}\,\tilde{\mathbf{h}}_{l,k}\right) \in \mathbb{C}^{M\times 1}, \tag{5}$$

where $\bar{\mathbf{G}}_l = \mathbf{a}_{\mathrm{RU}}(r_l)\mathbf{a}_{\mathrm{BS}}^{\mathrm{H}}(s)$ and $\bar{\mathbf{h}}_{l,k} = \mathbf{a}_{\mathrm{RU}}(v_{l,k})$ represent LoS components, $\tilde{\mathbf{G}}_l$ and $\tilde{\mathbf{h}}_{l,k}$ represent NLoS components, which follows the identically and independently distributed circularly-symmetric complex Gaussian distribution, while τ is the channel power gain at the reference distance of 1 m, κ denotes the path loss exponent, and R is the Rician factor.

Let s_k be the data symbol for the kth UE. The signal transmitted by the BS is described by

$$\mathbf{x} = \sum_{k=1}^{K} \sqrt{p_k}\,\mathbf{w}_k s_k, \tag{6}$$

where $\mathbf{W} = [\mathbf{w}_1,\ldots,\mathbf{w}_K]^{\mathrm{H}} \in \mathbb{C}^{K\times N}$ is the BS's active beamforming matrix with $\mathbf{w}_k \in \mathbb{C}^{N\times 1}$ and $\|\mathbf{w}_k\|^2 = 1$, $\forall k$, and $\mathbf{p} = [p_1,\ldots,p_K]^{\mathrm{T}} \in \mathbb{R}^{K\times 1}$ is the BS power allocation vector. Define $\boldsymbol{\Phi} = \{\boldsymbol{\Phi}_l\}_{\forall l\in\mathcal{S}_{\mathrm{A}}}$, where $\boldsymbol{\Phi}_l = \mathrm{diag}\{\varphi_{l,1},\ldots,\varphi_{l,M}\} \in \mathbb{C}^{M\times M}$ denotes the phase shifts matrix for the lth RIS-UAV, with $\varphi_{l,m} = \mathrm{e}^{j\theta_{l,m}}$, $\theta_{l,m} \in [0, 2\pi)$ and $m \in \mathcal{M} = \{1,\ldots,M\}$. The signal received at the kth UE can be expressed as

$$y_k = \sum_{l=1}^{L} \mathbf{h}_{l,k}^{\mathrm{H}}\boldsymbol{\Phi}_l\mathbf{G}_l\mathbf{x} + n_k, \tag{7}$$

where $n_k \sim \mathcal{CN}(0,\sigma_0^2)$ is the additive white Gaussian noise at the kth UE. Therefore, the signal-to-interference-plus-noise ratio at the kth UE is given by

$$\gamma_k = \frac{p_k\left|\sum_{l=1}^{L}\mathbf{h}_{l,k}^{\mathrm{H}}\boldsymbol{\Phi}_l\mathbf{G}_l\mathbf{w}_k\right|^2}{\sum_{i=1,i\neq k}^{K} p_i\left|\sum_{l=1}^{L}\mathbf{h}_{l,k}^{\mathrm{H}}\boldsymbol{\Phi}_l\mathbf{G}_l\mathbf{w}_i\right|^2 + \sigma_0^2}. \tag{8}$$

C. Optimization Problem Formulation

Following the previous analysis, the EE of RIS-UAVs assisted system is defined as

$$\eta_{\mathrm{EE}} = \frac{B\sum_{k=1}^{K}\log_2(1+\gamma_k)}{\xi\sum_{k=1}^{K} p_k + P_{\mathrm{B}} + KP_{\mathrm{UE}} + P_{\mathrm{R}} + LP_{\mathrm{h}}}. \tag{9}$$

Here B represents the transmission bandwidth and ξ denotes the reciprocal of the power amplifier efficiency at the BS. The circuit power consumption at the BS and each UE are P_{B} and P_{UE}, respectively, while the total RIS power consumption is given by $P_{\mathrm{R}} = LMP_{\mathrm{RIS}}$, with P_{RIS} being the power per RIS element. As the RIS-UAVs are deployed at fixed positions to provide continuous and stable relaying, no extra dynamic propulsion power is consumed for movement. Therefore, the hovering power P_{h} of each UAV is generally considered as a constant [12]. Accordingly, the optimization problem to maximize the system EE can be constructed as

$$\mathcal{P}1:\ \max_{\mathbf{p},\mathbf{W},\boldsymbol{\Phi}}\ \ \eta_{\mathrm{EE}}(\mathbf{p},\mathbf{W},\boldsymbol{\Phi}), \tag{10a}$$

$$\text{s.t.} \quad \sum_{k=1}^{K} p_k \leq P_{\max},\ p_k \geq 0,\ \forall k, \tag{10b}$$

$$\|\mathbf{w}_k\|^2 = 1,\ \forall k, \tag{10c}$$

$$|\varphi_{l,m}|^2 = 1,\ \forall l, m. \tag{10d}$$

III. Joint Optimization

A. Problem Transformation

Problem $\mathcal{P}1$ is a non-convex fractional program, which we address by applying the Dinkelbach method to transform it into a more tractable equivalent form. Let $P_{\mathrm{C}} = P_{\mathrm{B}} + KP_{\mathrm{UE}} + P_{\mathrm{R}} + LP_{\mathrm{h}}$, the maximal EE η_{EE}^* satisfies

$$B\sum_{k=1}^{K}\log_2\left(1+\gamma_k(\mathbf{p}^*,\mathbf{W}^*,\mathbf{\Phi}^*)\right)-\eta_{\mathrm{EE}}^*\left(\xi\sum_{k=1}^{K}p_k^*+P_{\mathrm{C}}\right)=0, \tag{11}$$

where $\mathbf{p}^*$, $\mathbf{W}^*$, $\mathbf{\Phi}^*$ and p_k^* are the optimal values of $\mathbf{p}$, $\mathbf{W}$, $\mathbf{\Phi}$ and p_k, respectively, which may be derived by solving the problem formulated in (11). A direct solution for η_{EE}^* from (11) is, however, unavailable. Therefore, we apply an iterative Dinkelbach algorithm to find η_{EE}^*. Specifically, at the i_{D}th iteration, we set η_{EE}^* as follows

$$\eta_{\mathrm{EE}}^{(i_{\mathrm{D}})} = \frac{B\sum_{k=1}^{K}\log_2\left(1+\gamma_k\left(\mathbf{p}^{(i_{\mathrm{D}}-1)},\mathbf{W}^{(i_{\mathrm{D}}-1)},\mathbf{\Phi}^{(i_{\mathrm{D}}-1)}\right)\right)}{\xi\sum_{k=1}^{K}p_k^{(i_{\mathrm{D}}-1)}+P_{\mathrm{C}}}, \tag{12}$$

where $\mathbf{p}^{(i_{\mathrm{D}}-1)}$, $\mathbf{W}^{(i_{\mathrm{D}}-1)}$, $\mathbf{\Phi}^{(i_{\mathrm{D}}-1)}$ and $p_k^{(i_{\mathrm{D}}-1)}$ are the results of $(i_{\mathrm{D}}-1)$th iteration, with $\mathbf{p}^{(0)}$, $\mathbf{W}^{(0)}$, $\mathbf{\Phi}^{(0)}$ and $p_k^{(0)}$ denoting the corresponding initial values. For a given η_{EE}^*, solving $\mathcal{P}1$ is equivalent to solving the following optimization

$$\mathcal{P}2:\ \max_{\mathbf{p},\mathbf{W},\mathbf{\Phi}} B\sum_{k=1}^{K}\log_2\left(1+\gamma_k(\mathbf{p},\mathbf{W},\mathbf{\Phi})\right)-\eta_{\mathrm{EE}}^*\left(\xi\sum_{k=1}^{K}p_k+P_{\mathrm{C}}\right),$$
$$\text{s.t.}\quad (10b),\ (10c),\ (10d)\ . \tag{13}$$

However, problem $\mathcal{P}2$ is non-convex owing to the linear fractional expression of $\gamma_k(\mathbf{p},\mathbf{W},\mathbf{\Phi})$. Note that B is a constant, hence is omitted for simplicity. By applying the Lagrangian dual transformation [8] and letting $\boldsymbol{\zeta}_k=\sum_{l=1}^{L}\mathbf{h}_{l,k}^{\mathrm{H}}\mathbf{\Phi}_l\mathbf{G}_l$, we can reformulate problem $\mathcal{P}2$ by introducing the auxiliary variable $\boldsymbol{\omega}=[\omega_1,\cdots,\omega_K]^{\mathrm{T}}$ as follows

$$\mathcal{P}3:\ \max_{\mathbf{p},\mathbf{W},\mathbf{\Phi},\boldsymbol{\omega}}\ \sum_{k=1}^{K}\log(1+\omega_k)-\sum_{k=1}^{K}\omega_k+F(\mathbf{p},\mathbf{W},\mathbf{\Phi},\boldsymbol{\omega}),$$
$$\text{s.t.}\quad (10b),\ (10c),\ (10d)\ , \tag{14}$$

where $F(\mathbf{p},\mathbf{W},\mathbf{\Phi},\boldsymbol{\omega})$ is given by

$$F(\mathbf{p},\mathbf{W},\mathbf{\Phi},\boldsymbol{\omega})=\sum_{k=1}^{K}\frac{(1+\omega_k)p_k\left|\boldsymbol{\zeta}_k\mathbf{w}_k\right|^2}{\sum_{i=1}^{K}p_i\left|\boldsymbol{\zeta}_k\mathbf{w}_i\right|^2+\sigma_0^2}-\eta_{\mathrm{EE}}^*\left(\xi\sum_{k=1}^{K}p_k+P_{\mathrm{C}}\right). \tag{15}$$

Given the optimization variables $\mathbf{p}$, $\mathbf{W}$ and $\mathbf{\Phi}$, problem $\mathcal{P}3$ can be shown to have a maximum value of ω_k when $\omega_k\geq 0$. The optimal ω_k can be updated as follows

$$\omega_k^*=\frac{p_k\left|\boldsymbol{\zeta}_k\mathbf{w}_k\right|^2}{\sum_{i=1,i\neq k}^{K}p_i\left|\boldsymbol{\zeta}_k\mathbf{w}_i\right|^2+\sigma_0^2}. \tag{16}$$

When $\boldsymbol{\omega}$ is fixed, problem $\mathcal{P}3$ can be reformulated as

$$\mathcal{P}4:\ \max_{\mathbf{p},\mathbf{W},\mathbf{\Phi}} F(\mathbf{p},\mathbf{W},\mathbf{\Phi}),\ \text{s.t.}\ (10b),\ (10c),\ (10d)\ . \tag{17}$$

Using the quadratic transform [8], we introduce an auxiliary variable $\boldsymbol{\delta}=[\delta_1,\ldots,\delta_K]^{\mathrm{T}}$ and reformulate problem $\mathcal{P}4$ as

$$\mathcal{P}5:\ \max_{\mathbf{p},\mathbf{W},\mathbf{\Phi},\boldsymbol{\delta}} F_1(\mathbf{p},\mathbf{W},\mathbf{\Phi},\boldsymbol{\delta}),\ \text{s.t.}\ (10b),\ (10c),\ (10d)\ , \tag{18}$$

where $F_1(\mathbf{p},\mathbf{W},\mathbf{\Phi},\boldsymbol{\delta}) = \sum_{k=1}^{K}2\sqrt{1+\omega_k}\mathrm{Re}\left\{\delta_k^{\dagger}\sqrt{p_k}\boldsymbol{\zeta}_k\mathbf{w}_k\right\} - \sum_{k=1}^{K}|\delta_k|^2\left(\sum_{i=1}^{K}p_i\left|\boldsymbol{\zeta}_k\mathbf{w}_i\right|^2+\sigma_0^2\right)-\eta_{\mathrm{EE}}^*\left(\xi\sum_{k=1}^{K}p_k+P_{\mathrm{C}}\right)$, and $\delta^{\dagger}$ is conjugate of δ.

When $\mathbf{p}$, $\mathbf{W}$ and $\mathbf{\Phi}$ are given, let $\frac{\partial F_1}{\partial \delta_k}=0$, the optimal δ_k can be updated as follows

$$\delta_k^*=\frac{\sqrt{(1+\omega_k)p_k\left|\boldsymbol{\zeta}_k\mathbf{w}_k\right|^2}}{\sum_{i=1}^{K}p_i\left|\boldsymbol{\zeta}_k\mathbf{w}_i\right|^2+\sigma_0^2}. \tag{19}$$

Thus, problem $\mathcal{P}2$ can be expressed as

$$\mathcal{P}6:\ \max_{\mathbf{p},\mathbf{W},\mathbf{\Phi},\boldsymbol{\omega},\boldsymbol{\delta}} J(\mathbf{p},\mathbf{W},\mathbf{\Phi},\boldsymbol{\omega},\boldsymbol{\delta}),$$
$$\text{s.t.}\quad (10b),\ (10c),\ (10d)\ , \tag{20}$$

where $J(\mathbf{p},\mathbf{W},\mathbf{\Phi},\boldsymbol{\omega},\boldsymbol{\delta}) = \sum_{k=1}^{K}\Big(\log_2(1+\omega_k)-\omega_k+2\sqrt{1+\omega_k}\,\mathrm{Re}\left\{\delta_k^{\dagger}\sqrt{p_k}\boldsymbol{\zeta}_k\mathbf{w}_k\right\}-|\delta_k|^2\left(\sum_{i=1}^{K}p_i\left|\boldsymbol{\zeta}_k\mathbf{w}_i\right|^2+\sigma_0^2\right)\Big) - \eta_{\mathrm{EE}}^*\left(\xi\sum_{k=1}^{K}p_k+P_{\mathrm{C}}\right)$. Next, We adopt the BCD method to alternately optimize $\mathbf{p}$, $\mathbf{W}$ and $\mathbf{\Phi}$.

B. Optimal BS Power Allocation

Given the BS beamforming matrix $\mathbf{W}$ and the RIS phase shifts matrix $\mathbf{\Phi}$, the BS power allocation optimization problem is formulated as

$$\mathcal{P}7:\ \max_{\mathbf{p},\boldsymbol{\omega},\boldsymbol{\delta}} J\left(\mathbf{p},\boldsymbol{\omega},\boldsymbol{\delta}\right),\ \text{s.t.}\ (10b)\ . \tag{21}$$

We alternatively update $\mathbf{p}$, $\boldsymbol{\omega}$ and $\boldsymbol{\delta}$. Specifically, given $\mathbf{p}$, the variables $\boldsymbol{\omega}$ and $\boldsymbol{\delta}$ are updated by (16) and (19). Given $\boldsymbol{\omega}$ and $\boldsymbol{\delta}$, problem $\mathcal{P}7$ becomes a convex problem with respect to $\mathbf{p}$. By applying the Karush-Kuhn-Tucker conditions, the optimal power allocation coefficient satisfies

$$p_k^*=\left\{\frac{\sqrt{1+\omega_k}\,\mathrm{Re}\{\delta_k^{\dagger}\,\boldsymbol{\zeta}_k\,\mathbf{w}_k\}}{\sum_{i=1}^{K}\left(|\delta_i|^2|\boldsymbol{\zeta}_i\mathbf{w}_k|^2\right)+\rho+\xi\eta_{\mathrm{EE}}^*}\right\}^2, \tag{22}$$

where ρ is the Lagrange multiplier for the power constraint (10b), which can be calculated via the bisection method.

C. Beamforming Optimization

Given $\mathbf{p}$ and $\mathbf{\Phi}$, $\mathcal{P}6$ becomes

$$\mathcal{P}8:\ \max_{\mathbf{W},\boldsymbol{\omega},\boldsymbol{\delta}} J\left(\mathbf{W},\boldsymbol{\omega},\boldsymbol{\delta}\right),\ \text{s.t.}\ (10c)\ . \tag{23}$$

We alternatively update $\mathbf{W}$, $\boldsymbol{\omega}$ and $\boldsymbol{\delta}$. Specifically, given $\mathbf{W}$, the variables $\boldsymbol{\omega}$ and $\boldsymbol{\delta}$ are updated according to (16) and (19). Given $\boldsymbol{\omega}$ and $\boldsymbol{\delta}$, we optimize the BS beamforming matrix $\mathbf{W}$. To facilitate this optimization, the constraint (10c) can be expressed in the Riemannian manifold form as

$$\mathcal{R}=\{\mathbf{W}\in\mathbb{C}^{K\times N}\mid \mathbf{E}_{K\times K}\circ(\mathbf{W}\mathbf{W}^{\mathrm{H}})=\mathbf{E}_{K\times K}\}, \tag{24}$$

where $\mathbf{E}_{K\times K}$ denotes the $K \times K$ identity matrix and $\circ$ denotes the Hadamard product. To obtain the stable solution of $J(\mathbf{W})$, the conjugate gradient method with the Polak–Ribiére update rule is adopted. The procedure for the i_cth Riemannian conjugate gradient direction is as follows.

1) Compute Euclidean gradient: At the i_cth iteration point $\mathbf{W}^{(i_\mathrm{c})}$, the Euclidean gradient is

$$\nabla J(\mathbf{W}^{(i_\mathrm{c})}) = \left[\frac{\partial J}{\partial \mathbf{w}_1^{(i_\mathrm{c})}}, \ldots, \frac{\partial J}{\partial \mathbf{w}_K^{(i_\mathrm{c})}}\right], \tag{25}$$

where

$$\frac{\partial J}{\partial \mathbf{w}_k^{(i_\mathrm{c})}} = \sqrt{(1+\omega_k)\, p_k}\, \delta_k^\dagger \boldsymbol{\zeta}_k - \sum_{k=1}^{K} |\delta_k|^2\, p_k \mathbf{w}_k^\mathrm{H} \boldsymbol{\zeta}_k^\mathrm{H} \boldsymbol{\zeta}_k. \tag{26}$$

2) Calculate Oblique gradient:

$$\begin{aligned}\mathrm{grad}J(\mathbf{W}^{(i_\mathrm{c})}) &= \nabla J(\mathbf{W}^{(i_\mathrm{c})}) \\ &- (\mathbf{E}_{K\times K} \circ \mathrm{Re}\{\mathbf{W}^{(i_\mathrm{c})}(\nabla J(\mathbf{W}^{(i_\mathrm{c})}))^\mathrm{H}\})\mathbf{W}^{(i_\mathrm{c})}.\end{aligned} \tag{27}$$

3) Search direction computation:

$$\mathbf{d}_\mathcal{R}^{(i_\mathrm{c})} = -\mathrm{grad}J(\mathbf{W}^{(i_\mathrm{c})}) + \alpha_\mathcal{R}^{(i_\mathrm{c})} \beta_\mathcal{R}(\mathbf{d}_\mathcal{R}^{(i_\mathrm{c}-1)}), \tag{28}$$

where $\alpha_\mathcal{R}^{(i_\mathrm{c})} = \frac{\nabla J^\mathrm{H}(\mathbf{W}^{(i_\mathrm{c})})(\nabla J(\mathbf{W}^{(i_\mathrm{c})}) - \beta_\mathcal{R}(\nabla J(\mathbf{W}^{(i_\mathrm{c}-1)})))}{\|\nabla J(\mathbf{W}^{(i_\mathrm{c}-1)})\|^2}$ and $\beta_\mathcal{R}(\mathbf{d}_\mathcal{R}^{(i_\mathrm{c}-1)}) = \mathbf{d}_\mathcal{R}^{(i_\mathrm{c}-1)} - (\mathbf{E}_{K\times K} \circ \mathrm{Re}\{\mathbf{W}^{(i_\mathrm{c})}(\mathbf{d}_\mathcal{R}^{(i_\mathrm{c}-1)})^\mathrm{H}\})\mathbf{W}^{(i_\mathrm{c})}$.

4) Determine step size and project: The Armijo backtracking line search is employed to determine the step size ν, then $\mathbf{W}^{(i_\mathrm{c}+1)}$ is updated and projected back onto Oblique manifold until the objective function converges

$$\mathbf{W}^{(i_\mathrm{c}+1)} = \left[\frac{\mathbf{w}_1^{(i_\mathrm{c})} + \nu \mathbf{d}_{\mathcal{R},1}^{(i_\mathrm{c})}}{\|\mathbf{w}_1^{(i_\mathrm{c})} + \nu \mathbf{d}_{\mathcal{R},1}^{(i_\mathrm{c})}\|_2}, \ldots, \frac{\mathbf{w}_K^{(i_\mathrm{c})} + \nu \mathbf{d}_{\mathcal{R},K}^{(i_\mathrm{c})}}{\|\mathbf{w}_K^{(i_\mathrm{c})} + \nu \mathbf{d}_{\mathcal{R},K}^{(i_\mathrm{c})}\|_2}\right]^\mathrm{H}, \tag{29}$$

where $\mathbf{w}_k^{(i_\mathrm{c})}$ and $\mathbf{d}_{\mathcal{R},k}^{(i_\mathrm{c})}$ are the kth column elements of $\mathbf{W}^{(i_\mathrm{c})}$ and $\mathbf{d}_\mathcal{R}^{(i_\mathrm{c})}$, respectively.

Given $\mathbf{p}$, $\mathbf{W}$, $\boldsymbol{\omega}$ and $\boldsymbol{\delta}$, we solve for the optimal $\boldsymbol{\Phi}$. Let $\mathbf{v}_{l,k,i} = \mathrm{diag}(\mathbf{h}_{l,k}^\mathrm{H})\mathbf{G}_l \mathbf{w}_i$, problem $\mathcal{P}6$ becomes

$$\min_{\underline{\boldsymbol{\varphi}}} \underline{\boldsymbol{\varphi}}^\mathrm{H} \mathbf{A} \underline{\boldsymbol{\varphi}} - 2\mathrm{Re}\left\{\underline{\boldsymbol{\varphi}}^\mathrm{H} \mathbf{b}\right\}, \text{ s.t. (10d)}, \tag{30}$$

where $\underline{\boldsymbol{\varphi}} = \mathrm{vec}(\widetilde{\boldsymbol{\varphi}}) \in \mathbb{C}^{ML\times 1}$, with $\widetilde{\boldsymbol{\varphi}} = [\boldsymbol{\varphi}_1, \ldots, \boldsymbol{\varphi}_L] \in \mathbb{C}^{M\times L}$ and $\boldsymbol{\varphi}_l = [\varphi_{l,1}, \ldots, \varphi_{l,M}]^\mathrm{H} \in \mathbb{C}^{M\times 1}$. Here, $\mathrm{vec}(\cdot)$ denotes the vectorization operation. Moreover, we define $\mathbf{A} = \sum_{k=1}^K |\delta_k|^2 \sum_{i=1}^K \underline{\mathbf{v}}_{k,i} \underline{\mathbf{v}}_{k,i}^\mathrm{H} p_i \in \mathbb{C}^{ML\times ML}$ and $\mathbf{b} = \sum_{k=1}^K \sqrt{(1+\omega_k)\, p_k}\, \delta_k^\dagger \underline{\mathbf{v}}_{k,k} \in \mathbb{C}^{ML\times 1}$, where $\underline{\mathbf{v}}_{k,i} = \mathrm{vec}(\widetilde{\mathbf{v}}_{k,i}) \in \mathbb{C}^{ML\times 1}$ and $\widetilde{\mathbf{v}}_{k,i} = [\mathbf{v}_{1,k,i}, \ldots, \mathbf{v}_{L,k,i}] \in \mathbb{C}^{M\times L}$. Next, we adopt the MACD method to update the phase shifts $\underline{\boldsymbol{\varphi}}$ iteratively. In the standard coordinate descent algorithm, the j_1th reflecting element is updated as

$$\underline{\boldsymbol{\varphi}}_{j_1}^* = \exp\left(j\angle\chi_{j_1}\right), \tag{31}$$

where $\chi_{j_1} = \mathbf{b}_{j_1} - \sum_{j_2=1, j_2\neq j_1}^{ML} \mathbf{A}_{j_1,j_2} \underline{\boldsymbol{\varphi}}_{j_2}$, $\mathbf{A}_{j_1,j_2}$ denotes the element of $\mathbf{A}$ at the j_1th row and j_2th column and $\mathbf{b}_{j_1}$ is the j_1th element of $\mathbf{b}$.

However, for large-scale RIS or strong-coupling channel scenarios, element-wise updates alone may suffer from slow convergence or oscillations. To address this issue, we introduce momentum factor $\Gamma \in [0, 1)$. Let $\widetilde{\underline{\boldsymbol{\varphi}}}_{j_1}^{(i_\mathrm{M}+1)} = e^{j\left(\angle(\chi_{j_1}^{(i_\mathrm{M})}) + \Gamma \Delta \underline{\boldsymbol{\varphi}}_{j_1}^{(i_\mathrm{M})}\right)}$, where $\Delta \underline{\boldsymbol{\varphi}}_{j_1}^{(i_\mathrm{M})} = \underline{\boldsymbol{\varphi}}_{j_1}^{(i_\mathrm{M})} - \underline{\boldsymbol{\varphi}}_{j_1}^{(i_\mathrm{M}-1)}$ represents the previous update direction of the j_1th element. The momentum term $\Gamma \Delta \underline{\boldsymbol{\varphi}}_{j_1}^{(i_\mathrm{M})}$ effectively accelerates convergence by guiding the current phase adjustment along past update direction. The procedure of our proposed algorithm is summarized in Algorithm 1.

Algorithm 1 The Proposed MACD Method for RIS Phase Shifts Optimization

1: **Initialize** $\mathbf{A}$, $\mathbf{b}$, $\underline{\boldsymbol{\varphi}}^{(0)}$, give maximum number of iterations I_max, Γ and tolerance ε, set $\Delta \underline{\boldsymbol{\varphi}}^{(0)} = 0$ and iteration index $i_\mathrm{M} = 0$.
2: **repeat**
3: Calculate $\chi_{j_1}^{(i_\mathrm{M})} = \mathbf{b}_{j_1} - \sum_{j_2=1, j_2\neq j_1}^{ML} \mathbf{A}_{j_1,j_2} \underline{\boldsymbol{\varphi}}_{j_2}^{(i_\mathrm{M})}$;
4: Update $\widetilde{\underline{\boldsymbol{\varphi}}}_{j_1}^{(i_\mathrm{M}+1)} = e^{j\left(\angle(\chi_{j_1}^{(i_\mathrm{M})}) + \Gamma \Delta \underline{\boldsymbol{\varphi}}_{j_1}^{(i_\mathrm{M})}\right)}$;
5: Update $\underline{\boldsymbol{\varphi}}_{j_1}^{(i_\mathrm{M}+1)} = \widetilde{\underline{\boldsymbol{\varphi}}}_{j_1}^{(i_\mathrm{M}+1)} / \|\widetilde{\underline{\boldsymbol{\varphi}}}_{j_1}^{(i_\mathrm{M}+1)}\|$;
6: Update difference: $\Delta \underline{\boldsymbol{\varphi}}_{j_1}^{(i_\mathrm{M}+1)} = \underline{\boldsymbol{\varphi}}_{j_1}^{(i_\mathrm{M}+1)} - \underline{\boldsymbol{\varphi}}_{j_1}^{(i_\mathrm{M})}$;
7: **Until** $\Delta \underline{\boldsymbol{\varphi}}_{j_1}^{(i_\mathrm{M}+1)} \le \varepsilon$ or $i_\mathrm{M} > I_\mathrm{max}$.
8: **Output** Optimal RIS phase shifts $\underline{\boldsymbol{\varphi}}_{j_1}^* = \underline{\boldsymbol{\varphi}}_{j_1}^{(i_\mathrm{M}+1)}$.

D. Algorithm Analysis

Regarding the optimization of RIS phase shifts, the majorization-minimization (MM) method entails a complexity of $\mathcal{O}(M^6L^3)$ [11], while the semi-definite relaxation (SDR) approach exhibits a complexity of $\mathcal{O}(M^6L^6)$ [7]. In contrast, our proposed MACD algorithm, detailed in Algorithm 1, achieves a substantially lower complexity of $\mathcal{O}(I_\mathrm{M}M^2L^2)$, where I_M, typically on the order of tens, denotes its iteration count. For the remaining subproblems, the BS power allocation algorithm requires $\mathcal{O}(I_\mathrm{b}K^2)$ operations, with I_b being the number of bisection search iterations, and the active beamforming algorithm incurs $\mathcal{O}(I_\mathrm{c}K^2N)$, where I_c represents the iterations of the oblique manifold conjugate gradient procedure. Consequently, the overall computational complexity of the joint optimization framework is $\mathcal{O}(I_\mathrm{D}I_\mathrm{B}(I_\mathrm{b}K^2 + I_\mathrm{c}K^2N + I_\mathrm{M}M^2L^2))$, with I_D and I_B denoting the iteration numbers of the outer Dinkelbach and inner BCD loops, respectively.

IV. Simulations

This section evaluates our proposed algorithm via simulations. The RIS-UAVs are deployed within a region centered at $(50, 0)$ m at a height of $H = 40$ m, with a radius $R_\mathrm{A} = 5$ m and $L = 3$ RIS-UAVs. The UE region is centered at $(100, 0)$ m with a radius $R_\mathrm{U} = 10$ m and the BS is located at $(0, 0)$ m. The channel gain at unit distance $\tau = 30$ dB, the path loss exponent $\kappa = 2$, the Rician fading factor $R = 10$ and the noise power $\sigma_0^2 = -80$ dBm. The transmission bandwidth $B = 1$ MHz, the reciprocal of the power amplifier efficiency at the BS is $\xi = 1.2$. Other parameters are set as follows: $P_\mathrm{B} = 100$ mW, $P_\mathrm{UE} = 20$ mW, $P_\mathrm{h} = 40$ mW and $P_\mathrm{RIS} = 1$ mW. Unless otherwise specified, the following parameters are used: the BS maximum transmit power $P_\mathrm{max} = 30$ dBm, the number of RIS elements $M = 10$, the number of BS antennas $N = 8$ and the number of UEs $K = 4$.

To compare with our proposed algorithm, we consider the following five benchmark schemes:

(1) **MM**: RIS phase shifts optimized via the MM algorithm.

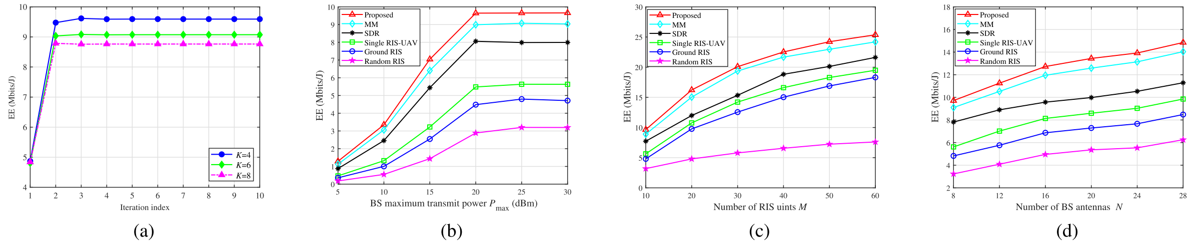

Fig. 2. (a) Convergence performance; (b) EE versus BS maximum transmit power $P_{\max}$; (c) EE versus number of RIS elements M; and (d) EE versus number of BS antennas N.

(2) **SDR**: RIS phase shifts optimized via the SDR algorithm.
(3) **Single RIS-UAV**: The number of RIS-UAVs is set to $L = 1$, while other parameters remain consistent with our proposed algorithm.
(4) **Ground RIS**: The RIS is positioned close to the ground, approximately 10 m above the UEs.
(5) **Random RIS**: The reflecting elements of the RIS adopt random phase shifts.

Fig. 2(a) illustrates the convergence performance of our proposed algorithm by plotting system EE against the outer Dinkelbach iteration count I_{D} for different numbers of UEs K. The algorithm converges within approximately 4 iterations. Furthermore, the system EE declines as K increases. This is because the growth in SE becomes slower than the linear increase in total UE circuit power consumption, i.e, KP_{UE}, ultimately lowers the overall EE.

Fig. 2(b) depicts the system EE versus the BS maximum transmit power $P_{\max}$ under different schemes. In all cases, EE initially rises and then gradually saturates as $P_{\max}$ increases. At low power levels, higher transmit power boosts the SE, yielding a rapid EE gain. Beyond $P_{\max} = 20$ dBm, however, the logarithmic nature of the SE function leads to diminishing returns, and further power increments bring negligible EE improvement. Compared to the MM and SDR benchmarks, our proposed scheme achieves EE gains of 7.37% and 19.67%, respectively.

Fig. 2(c) illustrates how the number of RIS elements M affects system EE across different schemes. For small M, increasing M yields notable passive beamforming gains, which improve the SE and consequently raise EE. Since SE follows a logarithmic function of M, in contrast to the linear growth of P_{R}, the EE improvement gradually slows as M increases. Hence, M should be chosen carefully to balance performance and power overhead.

Fig. 2(d) investigates the effect of the number of BS antennas N on system EE. Increasing N improves EE by providing greater spatial degrees of freedom and enhancing SE. However, due to the logarithmic relationship between SE and N, the EE gain diminishes as N grows. In comparison, both the single RIS-UAV and ground RIS setups rely on reflected paths, which limits their ability to exploit additional antennas. Consequently, their EE improves more gradually with larger N than our proposed RIS-UAVs assisted system.

V. Conclusion

This letter has investigated the joint optimization of BS power allocation, active beamforming and RIS phase shifts for RIS-UAVs assisted multiuser communication systems to maximize system EE. To tackle the non-convexity of this challenging problem, a Dinkelbach-based BCD algorithm framework has been applied to decompose the complex problem into three simpler subproblems, which are iteratively optimized. Moreover, a low-complexity MACD algorithm is introduced specifically for optimizing the RIS phase shifts. Simulation results have demonstrated that our proposed approach significantly enhances system EE compared to existing benchmark methods. Nevertheless, the lack of comparisons with DL/DRL baselines constitutes a limitation. In future work, we will focus on integrating our optimization framework with DL/DRL methods, while introducing dynamic UAV power models and trajectory optimization to achieve overall system EE.

References

[1] M. Ahmed et al., "Toward a sustainable low-altitude economy: A survey of energy-efficient RIS–UAV networks," *IEEE Internet Things J.*, vol. 12, no. 24, pp. 51951–51975, Dec. 2025.

[2] Z. Ning et al., "6G communication new paradigm: The integration of autonomous aerial vehicles and intelligent reflecting surfaces," *IEEE Commun. Surveys Tuts.*, vol. 27, no. 6, pp. 3382–3416, Dec. 2025.

[3] B. Shang, R. Shafin, and L. Liu, "UAV swarm-enabled aerial reconfigurable intelligent surface (SARIS)," *IEEE Wireless Commun.*, vol. 28, no. 5, pp. 156–163, Oct. 2021.

[4] Y. Ren, Z. Wang, X. Zhang, and G. Lu, "Energy efficiency maximization for aerial RIS-aided over-the-air federated learning," in *Proc. IEEE Wireless Commun. Netw. Conf. (WCNC)*, Apr. 2024, pp. 1–6.

[5] Y. Ye, S. Hu, W. Ni, and X. Wang, "Trajectory planning and transmission scheduling for UAV-borne RIS assisted energy-efficient uplink transmissions," *IEEE Trans. Intell. Transp. Syst.*, vol. 26, no. 10, pp. 17185–17193, Oct. 2025.

[6] B. Adhikari, A. S. Khwaja, M. Jaseemuddin, A. Anpalagan, and A. Nallanathan, "Energy efficient RIS-assisted UAV networks using twin delayed DDPG technique," *IEEE Trans. Wireless Commun.*, vol. 23, no. 12, pp. 18423–18439, Dec. 2024.

[7] L. Ge, H. Zhang, J.-B. Wang, and G. Y. Li, "Reconfigurable wireless relaying with multi-UAV-carried intelligent reflecting surfaces," *IEEE Trans. Veh. Technol.*, vol. 72, no. 4, pp. 4932–4947, Apr. 2023.

[8] B. Shang, E. S. Bentley, and L. Liu, "UAV swarm-enabled aerial reconfigurable intelligent surface: Modeling, analysis, and optimization," *IEEE Trans. Commun.*, vol. 71, no. 6, pp. 3621–3636, Jun. 2023.

[9] P. S. Aung, Y. M. Park, Y. K. Tun, Z. Han, and C. S. Hong, "Energy-efficient communication networks via multiple aerial reconfigurable intelligent surfaces: DRL and optimization approach," *IEEE Trans. Veh. Technol.*, vol. 73, no. 3, pp. 4277–4292, Mar. 2024.

[10] Y. Byun, H. Kim, S. Kim, and B. Shim, "Channel estimation and phase shift control for UAV-carried RIS communication systems," *IEEE Trans. Veh. Technol.*, vol. 72, no. 10, pp. 13695–13700, Oct. 2023.

[11] Y. Guo, Y. Liu, Q. Wu, Q. Shi, and Y. Zhao, "Enhanced secure communication via novel double-faced active RIS," *IEEE Trans. Commun.*, vol. 71, no. 6, pp. 3497–3512, Jun. 2023.

[12] Y. Ren et al., "Energy efficiency optimization for UAV distribution and resource allocation in NOMA and multi-UAV assisted wireless networks," *IEEE Open J. Commun. Soc.*, vol. 6, pp. 6142–6155, 2025.